

Atomistic Modeling of the Electrical Conductivity of Single-Walled Carbon Nanotube Junctions

Thomas R. Durrant,* Al-Moatasem El-Sayed, David Z. Gao, Thomas Rueckes, Gennadi Bersuker, and Alexander L. Shluger

Carbon nanotubes (CNTs) have many interesting properties that make them a focus of research in a wide range of technological applications. In CNT films, the bottleneck in charge transport is typically attributed to higher resistance at CNT junctions, leading to electrical transport characteristics that are quite different from individual CNTs. Previous simulations confirm this; however, a systematic study of transport across junctions is still lacking in the literature. Herein, density functional tight binding (DFTB) theory combined with the nonequilibrium Green's functions (NEGF) method is used to systematically calculate current across a range of CNT junctions. A random sampling approach is used to sample an extensive library of junction structures. The results demonstrate that the conductivity of CNT contacts depends on the overlap area between nanotubes and exponentially on the distances between the carbon atoms of the interacting CNTs. Two models based solely on the atomic positions of carbon atoms within the nanotubes are developed and evaluated: a simple equation using only the smallest C–C separation and a more sophisticated model using the positions of all C atoms. These junction current models can be used to predict transport in larger-scale simulations where the CNT fabric structure is known.

research over the past few decades. It has resulted in their use in a wide range of applications, including wearable, transparent and flexible electronics, gas sensing, catalysis, resistive switching, space exploration, and more.^[2,4–13] In many of these applications, a CNT network is fabricated as a film, synonymously referred to as a fabric. An example of the structure of a disordered film is shown in Figure 2 in the study by Lyons et al.^[14] Due to the complexity of the fabric structure, the desirable properties of a single nanotube do not directly translate into the characteristics of the CNT film as a whole. As a result, significant research has been devoted to understanding how the interaction between individual nanotubes affects electrical and mechanical properties of a CNT fabric.

Efforts have been made to understand the conductivity of CNT fabrics and they can be divided into two camps, those that parameterize larger-scale empirical

1. Introduction


First synthesized in significant quantities in the 1990s, carbon nanotubes (CNTs) have extremely desirable electronic, optical, and mechanical properties.^[1–3] Exploitation of their electronic, optical, and mechanical properties has, therefore, been a focus of

models^[14–16] and those that are based on CNT film structural models.^[17–20] In all these studies, the total resistance of the film is controlled by the relatively high electrical resistance of quantum–mechanical tunneling of electrons from one CNT to another. In contrast (at low voltages), individual CNTs behave as ballistic conductors, demonstrating quantized conductance

T. R. Durrant, D. Z. Gao
Department of Physics and Astronomy
University College London
Gower Street, London WC1E 6BT, UK
E-mail: thomas.durrant.14@ucl.ac.uk

T. R. Durrant, A.-M. El-Sayed, D. Z. Gao
Nanolayers Research Computing Ltd.
1 Granville Court, Granville Road, London N12 0HL, UK

A.-M. El-Sayed
Institute for Microelectronics
Technische Universität Wien
A-1040 Vienna, Austria

 The ORCID identification number(s) for the author(s) of this article can be found under <https://doi.org/10.1002/pssr.202200118>.

© 2022 The Authors. physica status solidi (RRL) Rapid Research Letters published by Wiley-VCH GmbH. This is an open access article under the terms of the Creative Commons Attribution License, which permits use, distribution and reproduction in any medium, provided the original work is properly cited.

DOI: 10.1002/pssr.202200118

D. Z. Gao
Department of Physics
NTNU
NO-7491 Trondheim, Norway

T. Rueckes
Nantero Inc.
25-B Olympia Avenue, Woburn, MA 01801, USA

G. Bersuker
The Aerospace Corporation
Los Angeles, CA 90245, USA

A. L. Shluger
Department of Physics and Astronomy
University College London
Gower Street, London WC1E 6BT, UK

A. L. Shluger
London Centre for Nanotechnology
University College London
Gower Street, London WC1E 6BT, UK

and high electrical conductivity^[21,22] with an experimentally measured electron free path of over 1 μm .^[23] This ensures that the contact resistance of CNT junctions is orders of magnitude higher than the intrinsic CNT resistance, as long as the individual CNTs are not so defective as to lose their intrinsic conductivity.^[14]

Measurements and simulations exploring charge transport properties of CNT contacts, such as other studies,^[24–26] have provided important insights into how they contribute to the film's conductivity. They have demonstrated that the electrical current through such junctions is sensitive to a combination of factors that control each junction's resistance, such as the physical separation, chirality, contact angle, overlap area, and the exact arrangement of carbon atoms at CNT junctions.^[24,26] However, accurately understanding and predicting the junctions' resistance is inherently challenging due to the high flexibility of nanotubes, leading to a wide range of possible junction structures. Despite their crucial role in the film conductivity, a systematic understanding of conductivity through CNT junctions has not yet been achieved.

In this study, the density functional tight binding method (DFTB) and the associated nonequilibrium Green's functions (NEGF) technique were employed to systematically calculate the current across pairs of nanotubes. A wide range of CNT–CNT contacts were generated using a random sampling approach to build an expansive library of junctions and their corresponding transport characteristics. These results demonstrated that the conductivity of CNT contacts depends linearly on the

overlap area between nanotubes and exponentially on the distances between the carbon atoms of the coupled CNTs. They were then used to parameterize a model that describes the total junction current based exclusively on the atomic positions of carbon atoms within participating CNTs. Two models were produced and evaluated: a simple model using only the smallest C–C separation and a more sophisticated model using the positions of all C atoms in the CNT pair. These computationally cheap junction current models can be used to quickly assess transport through complex CNT fabrics from their atomic structure.

2. Computational Methods

The structures of individual CNTs were specified by two chirality indices (n, m) which control both the radius and the electronic properties of the CNT. In this study, only metallic armchair CNTs with chiralities where the two indices are equal (n, n) were considered. Naturally, the electrical conductivity of semiconducting CNTs was lower than those reported here. In addition, only single-walled CNTs were considered, whereas CNTs in many applications were in fact multiwalled with smaller CNTs nested within larger ones. Finally, the ends of the nanotubes in the device regions were passivated by H atoms.

In CNT fabrics, the nanotube orientations can be highly disordered and their contacts can take on a wide range of different local geometries. Therefore, randomly sampled perturbations were applied to the junction structures to avoid systematic biases

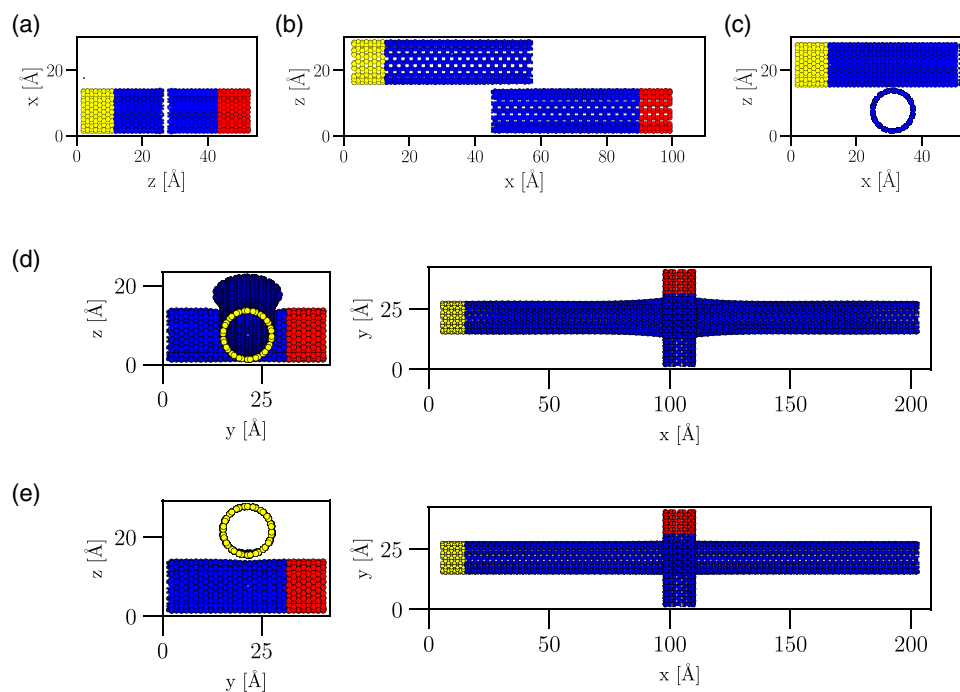


Figure 1. Template structures used in NEGF calculations of electrical current. The red, yellow, and blue regions represent the source, drain, and device regions, respectively. The three structures are: a) 756 atom tip-to-tip; b) 1620 atom parallel; and c) 1188 atom perpendicular. Random perturbations were applied to these structures, as shown in Table 1, to generate a diverse range of structures. The two nanotubes were oriented so that they were separated in the z -direction. Two additional structures were considered for comparison with experiment: d) 3490 atom coplanar (surface) junction structure with ends of two perpendicular CNTs lying in the same plane and e) 3490 atom equivalent noncoplanar (free space) junction, where the upper CNT is positioned above the plane.

Table 1. Random perturbations applied to the second tubes (those the drain region) in the template structures of Figure 1a–c to generate a diverse range of junction structures. All perturbations are given in Å. Random numbers are uniformly sampled from the interval given in square brackets and then applied to the relevant coordinates. The CNTs are also rotated around their axes to sample all available rotations.

	Tip to tip	Parallel	Perpendicular
Δx	–	[–28, 0]	[0, 2]
Δy	–	[0, 2]	[0, 2]
Δz	[–3, 0]	[–1, 0]	[–4, 0]

and sample a larger configuration space. The three template structures shown in Figure 1a–c were used as starting configurations and many random perturbations, as described in Table 1, were applied to generate a robust library of structures. CNT junctions were oriented so that the tubes were separated in the z-direction, as shown in Figure 1. The physical separation between CNTs was partially controlled by the random perturbation Δz . The shifts Δx and Δy were also sampled, as the CNTs were not always perfectly aligned in real fabrics. Finally, both tubes were rotated around their own axes. Due to the rotational symmetry of the nanotubes, it was only necessary to sample between 0° and $(360/n)^\circ$, where n is the chirality of the nanotube being rotated. The intent of the perturbations in Table 1 was not to sample all available possible structures but instead to provide a rich enough dataset for model construction. As a result, the perturbations themselves were not unique and could be extended to cover a larger range of configurations.

The atomic and electronic structures of CNT contacts were calculated using the DFTB+ electronic structure code with the 3OB set of Slater–Koster parameters to represent H, C, and O atoms.^[27,28] The many-body dispersion approach was used^[27,29,30] to describe van der Waals (vdW) interactions properly. As the vdW interaction strength increased, the electrical conductivity was also expected to increase.^[31] Geometry optimizations were carried out to a force tolerance of $5 \times 10^{-3} \text{ eV \AA}^{-1}$. The DFTB approach was not the only method available to study the electrical conductivity of CNT junctions and it would be useful to compare the performance of other methods to the structures released in this article in the future.

Within the NEGF approach, the simulated junctions were made up of three separate regions, as shown in Figure 1. They consisted of a device region (shown in blue) where the junction was located and two semi-infinite contact regions: the source (red) and drain (yellow). The device region was chosen to be large enough to recover a bulk-like electron density at the contacts which was required for accurate current calculations. The contact regions were each four unit cells long. The geometry of the device region in each structure in the library was optimized, while the contact regions remained fixed. A total bias of 0.5 V was then applied across the geometry optimized device region (–0.25 and 0.25 V to the contacts) and NEGF was used to calculate the resulting current through the whole junction. This 0.5 V bias voltage was in the low-voltage ohmic regime for CNTs. Currently, DFTB+ can only simulate device regions that are

aligned with the coordinate system’s axes and all structures were constructed with either parallel or perpendicular contact regions. In real fabrics, a distribution of angles would be observed between these two extremes. It is possible that the intermediate structures display different trends, although the present data did not suggest this as the parallel and perpendicular results displayed similar behavior. The overlap should increase continuously as CNTs are rotated from perpendicular to parallel arrangements.

3. Results

3.1. Method Validation

The properties of individual CNTs were calculated and compared to the published data^[21,32–34] to validate the methods employed in this study. A (9,9) chirality nanotube was used as a prototypical system. First, ballistic conduction observed for metallic CNTs^[21] was reproduced. As anticipated, the conductance of the CNT was found to be independent of the tube length, as it behaves like a 1D ballistic conductor, and was found to be $2G_0$, where G_0 is the conductance quantum. This results in a current of $7.75 \times 10^{-5} \text{ A}$ at the 0.5 V bias applied. The calculated work function of this nanotube was 4.75 eV, which is within the range of 4.7–5.05 eV that has been reported experimentally.^[32–34]

The methods employed were further evaluated by calculating current across a CNT junction to evaluate the nature of its conductance. Ohmic behavior was observed for bias voltages below 0.8 V, followed by a sudden nonohmic current increase at higher voltages, as shown in the I – V plot in Figure 2. This increase is caused by a greater availability of conduction channels deeper in the bands, away from the Fermi level, and is similar to previous theoretical calculations (e.g., Figure 4 in the study by Buldum et al.^[26]) and to the experimental data.^[24,25]

There is a mismatch between theoretical calculations of the conductance of perpendicular junctions and those measured

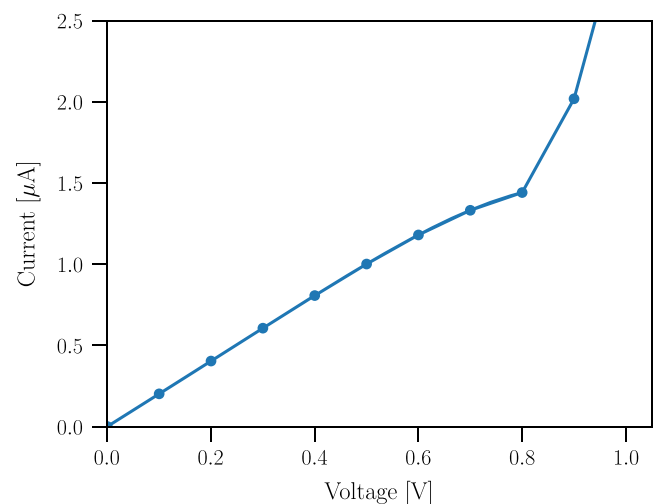


Figure 2. Current–voltage sweep for a characteristic CNT junction evaluated using NEGF. Ohmic behavior was observed below 0.8 V. The structure used was a typical (9,9) parallel junction.

experimentally.^[26] It has been suggested by Buldum and Lu^[26] that the presence of an underlying substrate holds the CNT junction spatially closer together than in the case of CNT junctions in free space and that this leads to higher current in the experiments. We investigated how the presence of an underlying substrate or other CNTs could result in deformed or confined junctions that are spatially closer together than their ideal vdW separation. The difference between coplanar and non-coplanar junctions was investigated, as shown in Figure 1d–e. In a cross-bar arrangement deposited on a substrate, one of the CNTs would be deformed around the junction area as it overlaps with the nanotube below. This geometry was reproduced by holding the ends of the nanotubes fixed in the same plane (coplanar geometry) and displacing one of the CNTs above the other at the crossing point. The observed fivefold increase of the junction current to 1.23×10^{-6} A is in agreement with the experimentally measured current of $1.4\text{--}5.5 \times 10^{-6}$ A.^[24] Although encouraging, these results should be treated as semi-quantitative as the computational models used (as shown in Figure 1d–e) were too small to fully describe the high strain junction structure produced, and hence full convergence of the total current with respect to the size of the model was not achieved. Explicitly modeling the interactions between a CNT junction and a substrate is, however, beyond the scope of this study.

When forming a CNT junction, there are many configurations that can be created, as the nanotube is not an ideal cylinder but consists of hexagons of carbon atoms on its surface. For example, in Figure 3, a junction was formed from two parallel CNTs (like that shown in Figure 1b), where one of them was rotated around its own axis. The resultant relative energies and the electrical current shown in Figure 3 demonstrate a strong dependence on the rotation angle. The highest conductivity in Figure 3 is achieved for $\theta_B = 0^\circ$ and 40° , which correspond to full alignment between the carbon atoms in both structures; that is, the tubes are a mirror image of each other. In this case, carbon atoms in the second tube are exactly aligned in x and y with the

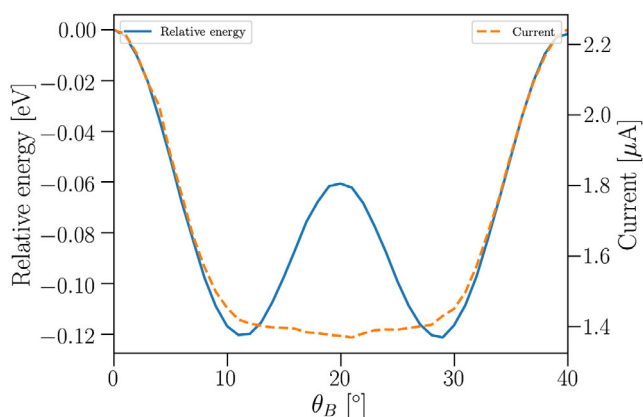


Figure 3. Rotational dependence of the current through a parallel junction. In a parallel CNT junction, one of the CNTs is rotated around its axis by the rotation angle θ . The angles $\theta = 0^\circ$ and $\theta = 40^\circ$ correspond to the “in registry” configuration, where the C atoms from the individual nanotubes are mirror images of each other. The energy relative to $\theta = 0^\circ$ is shown on the left y-axis, and the electrical current is shown on the right y-axis.

neighboring atoms in the first and are only separated in the z direction. In the literature, such structures are termed ‘in registry’ and are known to form the most conductive contacts between CNTs.^[26] Note that these structures are not the lowest-energy configurations available and that the energy cost of CNT rotation is low.

3.2. Conductivity and Current through Library of Junctions

A large library of (9,9) chirality junction structures was produced to systematically study the role of geometry on junction conductance. Randomly generated junctions that resulted in a total current of less than 1×10^{-11} A were excluded from the dataset, as numerical significance was lost below this value. Once these low-current structures were discarded, the final library contained 185 tip-to-tip, 240 parallel, and 195 perpendicular junctions (see Figure 1a–c).

The geometries of all CNT junctions from this library were optimized as described in the Experimental Section. The major effect of the optimization was on the smallest separation between the CNTs, shown in Figure 4 for (9,9) CNTs. There is only a weak vdW interaction between the well separated tubes; however, if the separation was small enough, the CNTs bent to reduce the total energy of the system and reach a minimum separation of around 2.9 Å, as shown in Figure 4. The same behavior was observed for all the chiralities studied. It should be noted from our results that the equilibrium separation between the tubes is chirality dependent, with tubes of larger radii demonstrating a larger equilibrium distance. This property has been predicted in previous theoretical calculations of CNTs in a square lattice and is understood to arise due to a balance of the vdW interaction and stress energy required to deform the tubes at their contact sites.^[35]

3.2.1. A Junction Current Model

The transport mechanism at CNT–CNT junctions is understood to be quantum–mechanical tunneling.^[14–20] In the low-voltage regime, the tunneling current density, J , between two

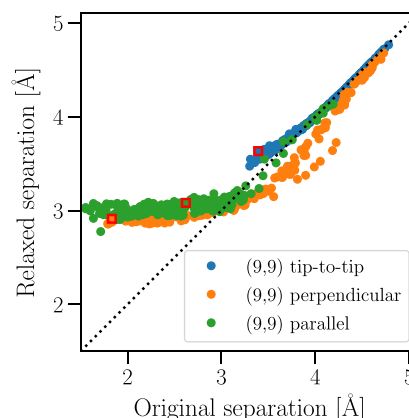


Figure 4. Correlation of the shortest C–C separations between paired CNTs before (x -axis) and after (y -axis) geometry optimization. Squares denote the template structures.

infinite conducting films with an intermediate barrier can be approximated as^[36]

$$J = \frac{(2m\bar{\phi})^{\frac{1}{2}}}{\Delta r} \left(\frac{e}{\hbar}\right)^2 V \exp\left(-\frac{4\pi\beta\Delta r}{\hbar}(2m\bar{\phi})^{\frac{1}{2}}\right) \quad (1)$$

where $\bar{\phi}$ is the tunneling barrier height, V is the voltage drop over the barrier, m is the mass of an electron, Δr is the barrier thickness, \hbar is Planck's constant, and e is the electron charge. A correction factor β that depends on the exact shape of the barrier is typically taken to be $\beta \approx 1$.^[36] This approximation serves as a good starting point for estimating the current through CNT junctions. It is clear that the barrier thickness Δr plays a critical role, as the total current is exponentially dependent on this parameter.

To simplify the analysis, some of the above terms can be combined to produce the fit parameters as

$$B = (2m\bar{\phi})^{\frac{1}{2}} \left(\frac{e}{\hbar}\right)^2 S \quad \text{and} \quad C = \frac{4\pi\beta}{\hbar} (2m\bar{\phi})^{\frac{1}{2}} \quad (2)$$

The contact area S has also been introduced to convert the final expression from current density to total current. The barrier thickness Δr can be approximated as the distance between two carbon nuclei where tunneling takes place. This will slightly overestimate the barrier thickness, as the electrons associated with the carbon atom are distributed over a larger volume. In principle, this error could be reduced by introducing another fit parameter and allowing a systematic reduction of the barrier. However, this was observed to provide only a marginal improvement.

From this point, two primary types of model are constructed. First, as the tunneling process described in Equation (1) is exponentially dependent on the separation, the total current will be dominated by the shortest value of Δr available. Hence, the simplest model that can be constructed is to assume that only the shortest distance between carbon atoms in two different CNTs (r_{\min}) will be important. In this case, the model will simply be

$$I = BV \frac{\exp(-Cr_{\min})}{r_{\min}} \quad (3)$$

where the value of r_{\min} is the smallest C–C separation between the two CNTs. The parameters B and C can be interpreted as fitting parameters.

To fit models, the mean of the absolute relative errors, defined as $\varepsilon = |I_{\text{model}} - I_{\text{dftb}}|/I_{\text{dftb}}$, was minimized. This ensured that both high- and low-current structures were given equal importance and avoided high-current structures from dominating the fit. The fit of Equation (3) to the NEGF data is shown in **Figure 5a**. It only incorporates the details of the local arrangement of carbon atoms at the junction in an indirect way: higher registry structures (where the carbon atoms line up) have a stronger vdW interaction and hence r_{sep} is smaller.

As shown in **Figure 5a**, the calculated current through the junctions increases with decreasing the C–C distance r_{\min} for all three of the junction types, as expected. This fit is more effective for the tip-to-tip and perpendicular junctions, but the description of the parallel junctions is not as good. The current through parallel junctions with a separation larger than 3.3 Å tends to be underestimated. On the other hand, the current through parallel junctions with lower separation is overestimated.

The model in Equation (3) assumes that the total conduction is approximated by tunneling through a single point of contact between the two CNTs. This can be expected to fail as the size of the contact area between two nanotubes is increased, and the conduction takes place over several sites where the carbon atoms are close enough for electrons to tunnel successfully. To incorporate this effect, the conduction should be modeled as a sum over all available conductive pathways. An appropriate sum to construct is

$$M = \sum_i \sum_j \frac{\exp(-Cr_{ij})}{r_{ij}} \quad (4)$$

where the position of each carbon atom i in the first nanotube and the position of each carbon atom j in the second nanotube

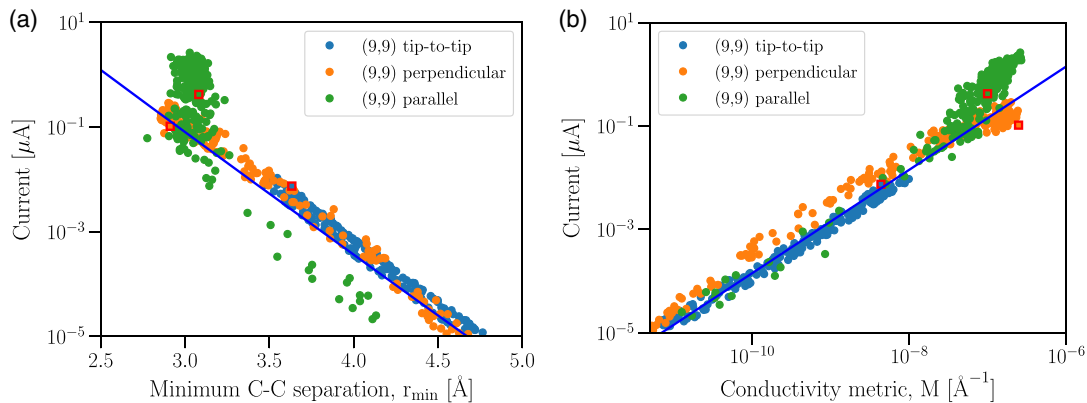


Figure 5. a) Fit of Equation (3) to the NEGF calculations. This simple model only uses the smallest distance between carbon atoms in different nanotubes. The fit shown is $B = 2.15 \text{ \AA}\Omega^{-1}$ and $C = 5.14 \text{ \AA}^{-1}$. The mean absolute relative error is 66%. b) Fit of Equation (5). This model uses information about the distances between every pair of carbon atoms, where one atom in the first pair is taken from the first nanotube and the second is taken from the second nanotube. The fit shown is $B = 2.49 \text{ \AA}\Omega^{-1}$ and $C = 5.76 \text{ \AA}^{-1}$. The mean absolute relative error is 46%. Squares denote the template structures.

is summed over. The summation M is termed “conductivity metric” in this article. Note that this is not just geometric like r_{min} but already includes the fit parameter C . This leaves the total current defined as

$$I = MBV \quad (5)$$

which produces a second model, a linear relationship that can be fitted to the data. Note the formal similarity between Equation (3) and (5) to Ohm’s law.

The fit of Equation (5) to the NEGF data is shown in Figure 5b. As mentioned earlier, the tip-to-tip structures were the least conductive, on average. It can be seen that they underperform in the general fit to the available data. Although these junctions do not require the conducting electrons to change their momentum (as in the perpendicular cases), the C–H groups that terminate the nanotubes prevent the carbon atoms in the junctions from getting closer together. A wider range of currents can be produced by the perpendicular junctions, depending on the separation between the nanotubes. Their conductivities are in reasonable agreement with the fit, with the current being slightly underestimated for low-conductivity metric and slightly overestimated for larger values. The parallel junctions are more conductive than the other types of junctions considered so far. They tend to be more conductive than the fit would suggest, a trend that is more prominent for larger values of the conductivity metric M .

The fit in Figure 5b remains approximate. This is to be expected as the model is too simplistic to fully capture the details of the tunneling process. In particular, the quasi-1D approximation in Equation (1) reduces the 3D tunneling problem to a simpler 1D problem. It was, furthermore, assumed that the tunneling barrier $\bar{\phi}$ is independent of the local structure. In principle, these assumptions can be addressed, but the complexity of the model would have to be greatly increased. We note that our data show that CNT–CNT junctions are highly variable and that even very structurally similar junctions can have quite different electrical conductivities.

The error in the fit in Figure 5b could be reduced by adding a nonlinear term to the fit. However, maintaining a linear relationship between the conductivity metric and the total current is

certainly justified by the available experimental data,^[37] which displays complex but approximately linear current dependency on the overlap length of CNT contacts. This same linear trend is observed in the DFTB+ data shown in Figure 6a. In these calculations, the overlap length is calculated as the distance in the x -direction (as labeled in Figure 6b,c) between the furthest atom in the first CNT from its contact region and the furthest atom in the second CNT from its contact region. The positive values imply that the parallel tubes overlap and the negative values imply that there is a separation in the x -direction between the CNTs. The scatter plot in Figure 6a shows how variable the conductivity of structurally similar CNT–CNT junctions can be. As summarized in Table 1, five random perturbations were applied to the structures. Only the perturbation Δx directly affects the overlap length, the remaining four perturbations introduce high structural variability and hence the observed high current variability. The model constructed is less accurate for these high overlap structures and further work is required in the future to better understand their conductivity.

The linear trend shown in Figure 6a was experimentally observed^[37] for overlap lengths greater than 80 Å, which is longer than that calculated using available computational resources. The current must saturate eventually as it is not sensible for the CNT–CNT contact to have a lower resistance than an individual unbroken CNT would. The length scale at which this saturation occurs remains an interesting, unanswered question.

3.2.2. Role of CNT Diameter

Now, we address the effect of nanotube diameter, or equivalently chirality, on junction conductivity. Changing the chirality of the CNTs modifies the junctions directly but also leads to greater changes in conductivity than would be expected due to the structural changes alone. Perpendicular junctions similar to the previous section were generated for chiralities in the range (6,6)–(12,12). Some of the chiralities considered are shown in Figure 7a. In these comparisons, the conductivity metric defined in Equation (4) is used again, and the fit parameter C is held fixed at the value that was previously established in the fit shown in Figure 5b. The simulations demonstrate that, as the chirality

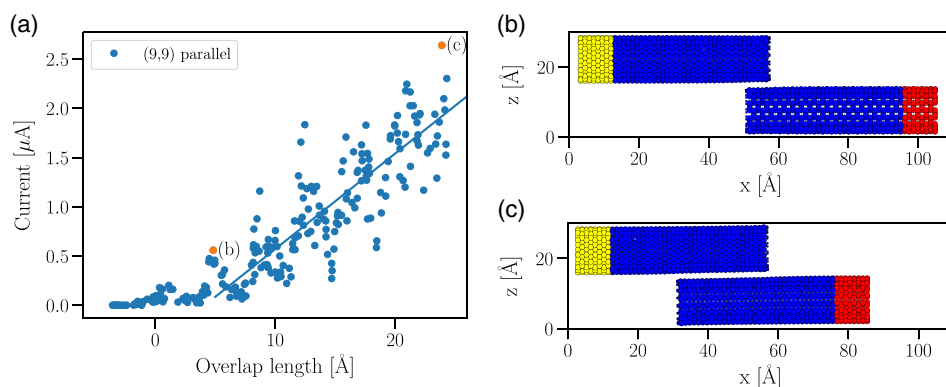


Figure 6. a) Relationship between electrical current and overlap length for the parallel (9,9) junctions considered. A linear trend is observed for the larger overlaps. A linear fit of $Px + Q$ is shown to the calculations, where the overlap length was greater than 5 Å. The fit parameters are $P = 0.097 \mu\text{A} \text{Å}^{-1}$, $Q = -0.40 \mu\text{A}$. Two points are highlighted in orange, and b,c) their geometries. The indicated junctions have overlap lengths of 4.84 and 23.09 Å, respectively.

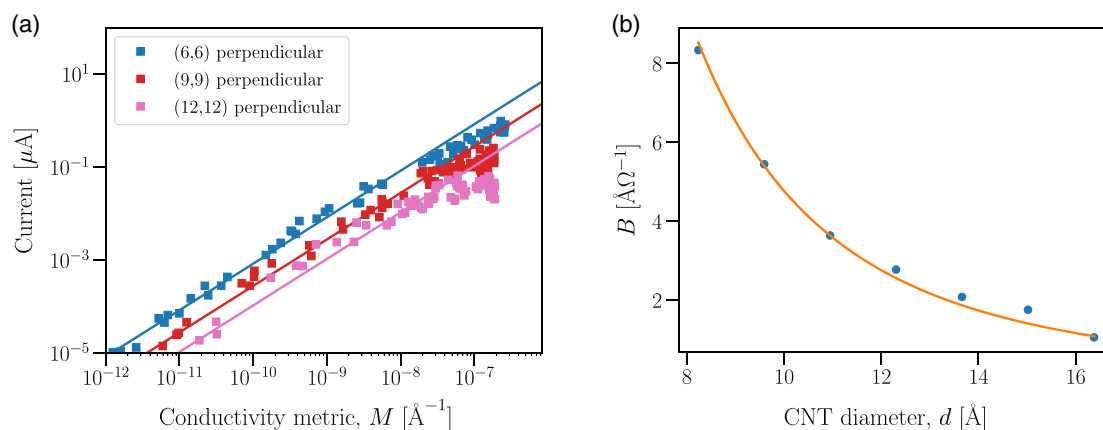


Figure 7. a) Relationship between electrical current and conductivity metric for the perpendicular (6,6), (9,9), and (12,12) junctions considered. A fit of Equation (5) to the individual datasets is shown. b) Fit of Equation (6) to the extracted B values for the various chiralities considered. In the fit, $D = 9.54 \times 10^3 \text{\AA}^4 \Omega^{-1}$. As in the rest of the article, only metallic armchair CNTs were considered.

of the nanotubes increases, the current decreases for similar values of M . The diameter of the nanotubes in these calculations, which is determined by the chirality, therefore plays an important role in determining the electrical conductivity of the junctions formed.

A linear relationship between the conductivity metric and the total electrical current through the junction persisted for the various chiralities considered. Again, this linear approximation was less successful for high values of the conductivity metric. This problem was more apparent as the radius of the CNTs increased. To make a systematic comparison between the various sizes, the value of the C parameter in Equation (5b) was fit to the data in the linear regime where $M [\text{\AA}^{-1}] < 1 \times 10^{-8}$.

An inverse cubic fit to the CNT diameter was found to be the best power law fit to the available data. To include this dependence in the model, the current fit with Equation (5) can be modified so that the value of B depends on the nanotube diameter d .

$$B = \frac{D}{d^3} \quad (6)$$

where D is a further fitting parameter. This inverse cubic fit to the diameter of the CNTs is shown in Figure 7b. The model fits the data fairly well, demonstrating the reduction in conductivity with increasing diameter. It is important to realize that the calculation of the conductivity metric M already incorporates important structural differences in the local junction structures as the size of the CNTs increases. However, the dependence illustrated in Figure 7b is an important additional effect that is not captured by the geometric features present in the definition of M .

The conductivity's dependence on diameter has been previously noted by Buldum and Lu,^[26] who argued that this can be explained by analyzing the change in contact area with respect to the tube's surface area as the diameter increases. The ballistic channel associated with conduction is located along the entire circumference of the nanotube. As the diameter of the nanotubes increases, the circumference increases more quickly than the

contact area at the nanotube junction.^[26] This hypothesis is consistent with the data reported here.

It should be emphasized that this expansion of the model is more empirical than the previous models presented, as there is no derivation of the inverse cubic dependence and this diameter dependence should be seen as approximate. It is clear that conductivity of similar junctions decreases with diameter, and this expression is provided as an approximate model of this effect.

Combining Equation (5) and (6) leads to a comprehensive expression

$$I = \frac{D}{d^3} V \sum_i \sum_j \frac{\exp(-C r_{ij})}{r_{ij}}, \quad (7)$$

which contains two fitting parameters, D and C .

4. Conclusion

The high structural variability of nanotube junctions greatly increases the complexity of predicting and understanding their electrical properties. In this work, a general approach was outlined where randomized structural sampling was used to generate an extensive library of nanotube junctions. Then, the DFTB/NEGF approach was used to evaluate the electrical current through the structures, demonstrating that the electrical current is highly variable with respect to the atomistic structure at the junction. The approach taken is not limited to CNTs and such an approach could be used for other similar systems, potentially allowing the systematic comparison of varied types of nanowires in the future.

The correspondence of calculated perpendicular (crossbar) junctions to experimental reported data was explored. Our results support the earlier suggestions^[26] that the measured currents are higher than those calculated for freestanding perpendicular junctions due to the interactions of the CNTs with the substrate acting to hold the CNTs closer together at their contact.

Two main models were proposed to fit the calculated data. First, a simplified model is based on the separation distance

Table 2. Overview of the conductivity models produced in this article, summarizing the recommended parameters.

Definition	Description	Parameters
Equation (3)	Separation model for (9,9)	$B = 2.15 \text{ \AA}\Omega^{-1}$, $C = 5.10 \text{ \AA}^{-1}$
Equation (5)	Atomistic model for (9,9)	$B = 2.49 \text{ \AA}\Omega^{-1}$, $C = 5.76 \text{ \AA}^{-1}$
Equation (7)	Atomistic model for (n,n)	$D = 9.54 \times 10^3 \text{ \AA}^4\Omega^{-1}$, $C = 5.76 \text{ \AA}^{-1}$

between CNTs in a junction where the current depends exponentially on the inter-CNT distance. This model can be employed when atomic details are not available, but it fails for CNTs with large overlap area. A more complex model accounting for individual positions of all carbon atoms in contacting CNTs is better able to describe large contacts in the parallel CNT configuration. It was also demonstrated that the conductivity of CNT junctions decreases with increasing chirality (diameter) and the second model was extended to incorporate this effect. To summarize the models that have been developed and fit in this work, their parameters are collected in **Table 2**.

Although an improved description of the data is achieved with the conductivity metric M rather than just the C–C separation r_{\min} , greater discrepancies are still observed for the highly conductive structures with parallel aligned CNTs. As a general trend, the fitted model seems less reliable when the contact area between CNTs is larger. The structures in this article demonstrate electrical conductivity across five orders of magnitude and future work is required to better understand the conductivity of parallel structures with high physical overlap.

The models and results presented in this article enable the approximate electrical resistance between two CNTs to be calculated based only on structural information, rather than requiring expensive electronic structure simulations. In particular, these models should enable electronic resistances of individual CNT–CNT contacts to be included into atomistic MD simulations of realistic CNT fabrics including thousands of CNTs. The models and data presented can also be used to parameterize other types of larger-scale models. Although CNT–CNT junctions are highly variable both in terms of their structure and in terms of their electrical conductivity, the results collected in this article should help to bridge the gap from smaller-scale electronic structure calculations to larger-scale structural models of CNT fabrics and lead to an improvement of the understanding of the electrical properties of these fascinating materials.

Acknowledgements

T.R.D., A.M.E., D.Z.G., and A.L.S. would like to thank Leonid Zhigilei and Alexey Volkov for valuable discussions. T.R.D. and A.L.S. acknowledge funding by the Engineering and Physical Sciences Research Council, grant no. EP/R034540/1EP/R034540/1, via our membership of the UK's HEC Materials Chemistry Consortium, which is funded by EPSRC (EP/L000202/1EP/L000202). This work used the ARCHER UK National Supercomputing Service (<http://www.archer.ac.uk>). The authors are grateful to the UK Materials and Molecular Modelling Hub for computational resources, which was partially funded by EPSRC (EP/P020194/1EP/P020194/1 and EP/T022213/1EP/T022213/1).

Conflict of Interest

The authors declare no conflict of interest.

Data Availability Statement

The data that support the findings of this study are openly available in UCL research data repository at [<http://doi.org/10.5522/04/19845523>], reference number [REF].

Keywords

amorphous fabrics, carbon nanotubes, electron transport

Received: March 26, 2022

Revised: May 27, 2022

Published online:

- [1] S. Iijima, *Nature* **1991**, 354, 56.
- [2] S. Iijima, T. Ichihashi, *Nature* **1993**, 363, 603.
- [3] M. Monthieux, V. L. Kuznetsov, *Carbon* **2006**, 44, 1621.
- [4] T. Rueckes, K. Kim, E. Joselevich, G. Y. Tseng, C. L. Cheung, C. M. Lieber, *Science* **2000**, 289, 94.
- [5] X. Zhang, W. Lu, G. Zhou, Q. Li, *Adv. Mater.* **2020**, 32, 1902028.
- [6] D. S. Bethune, C. H. Klang, M. S. de Vries, G. Gorman, R. Savoy, J. Vazquez, R. Beyers, *Nature* **1993**, 363, 605.
- [7] M. S. Dresselhaus, G. Dresselhaus, P. C. Eklund, *Science of Fullerenes and Carbon Nanotubes* Elsevier, Amsterdam, Netherlands **1996**.
- [8] T. Zhang, S. Mubeen, N. V. Myung, M. A. Deshusses, *Nanotechnology* **2008**, 19, 332001.
- [9] Y. Chai, Y. Wu, K. Takei, H.-Y. Chen, S. Yu, P. C. H. Chan, A. Javey, H. S. P. Wong, In *Inter. Electron Devices Meeting*, IEEE, Manhattan, NY **2010** pp. 9.3.1–9.3.4.
- [10] M. V. Il'ina, O. I. Il'in, Y. F. Blinov, V. A. Smirnov, A. S. Kolomytsev, A. A. Fedotov, B. G. Konoplev, O. A. Ageev, *Carbon* **2017**, 123, 514.
- [11] P. Serp, M. Corrias, P. Kalck, *Appl. Catal., A* **2003**, 253, 337.
- [12] B. Damirchi, M. Radue, K. Kanhaiya, H. Heinz, G. M. Odegard, A. C. van Duin, *J. Phys. Chem. C* **2020**, 124, 20488.
- [13] D. C. Gilmer, T. Rueckes, L. Cleveland, *Nanotechnology* **2018**, 29, 134003.
- [14] P. E. Lyons, S. De, F. Blighe, V. Nicolosi, L. F. C. Pereira, M. S. Ferreira, J. N. Coleman, *J. Appl. Phys.* **2008**, 104, 044302.
- [15] P. N. Nirmalraj, P. E. Lyons, S. De, J. N. Coleman, J. J. Boland, *Nano Lett.* **2009**, 9, 3890.
- [16] E. Snow, J. Novak, P. Campbell, D. Park, *Appl. Phys. Lett.* **2003**, 82, 2145.
- [17] S. Kumar, J. Y. Murthy, M. A. Alam, *Phys. Rev. Lett.* **2005**, 95, 066802.
- [18] T. Tarlton, J. Brown, B. Beach, P. A. Derosa, *Composites, Part B* **2016**, 100, 56.
- [19] T. Tarlton, E. Sullivan, J. Brown, P. A. Derosa, *J. Appl. Phys.* **2017**, 121, 085103.
- [20] L. Jin, A. Chortos, F. Lian, E. Pop, C. Linder, Z. Bao, W. Cai, *PNAS* **2018**, 115, 1986.
- [21] S. Frank, P. Poncharal, Z. Wang, W. A. de Heer, *Science* **1998**, 280, 1744.
- [22] C. T. White, T. N. Todorov, *Nature* **1998**, 393, 240.
- [23] J.-Y. Park, S. Rosenblatt, Y. Yaish, V. Sazonova, H. Üstünel, S. Braig, T. A. Arias, P. W. Brouwer, P. L. McEuen, *Nano Lett.* **2004**, 4, 517.

- [24] M. S. Fuhrer, J. Nygård, L. Shih, M. Forero, Y.-G. Yoon, M. S. C. Mazzoni, H. J. Choi, J. Ihm, S. G. Louie, A. Zettl, P. L. McEuen, *Science* **2000**, 288, 494.
- [25] M. Fuhrer, A. K. Lim, L. Shih, U. Varadarajan, A. Zettl, P. L. McEuen, *Physica E* **2000**, 6, 868.
- [26] A. Buldum, J. P. Lu, *Phys. Rev. B* **2001**, 63, 161403.
- [27] B. Hourahine, B. Aradi, V. Blum, F. Bonafé, A. Buccheri, C. Camacho, C. Cevallos, M. Y. Deshayé, T. Dumitrică, A. Dominguez, S. Ehlert, M. Elstner, T. van der Heide, J. Hermann, S. Irle, J. J. Kranz, C. Köhler, T. Kowalczyk, T. Kubař, I. S. Lee, V. Lutsker, R. J. Maurer, S. K. Min, I. Mitchell, C. Negre, T. A. Niehaus, A. M. N. Niklasson, A. J. Page, A. Pecchia, G. Penazzi, et al., *J. Chem. Phys.* **2020**, 152 124101.
- [28] M. Gaus, A. Goez, M. Elstner, *J. Chem. Theory Comput.* **2013**, 9, 338.
- [29] A. Tkatchenko, R. A. DiStasio, R. Car, M. Scheffler, *Phys. Rev. Lett.* **2012**, 108, 236402.
- [30] A. Ambrosetti, A. M. Reilly, R. A. DiStasio Jr, A. Tkatchenko, *J. Chem. Phys.* **2014**, 140, 18A508.
- [31] X.-K. Chen, X.-Y. Hu, P. Jia, Z.-X. Xie, J. Liu, *Int. J. Mech. Sci.* **2021**, 206, 106576.
- [32] P. Liu, Q. Sun, F. Zhu, K. Liu, K. Jiang, L. Liu, Q. Li, S. Fan, *Nano. Lett.* **2008**, 8, 647.
- [33] M. Shiraishi, M. Ata, *Carbon* **2001**, 39, 1913.
- [34] S. Suzuki, Y. Watanabe, Y. Homma, S.-Y. Fukuba, S. Heun, A. Locatelli, *Appl. Phys. Lett.* **2004**, 85 127.
- [35] V. Smirnov, L. Manevitch, *Dokl. Phys.* **2019**, 64, 218.
- [36] J. G. Simmons, *J. Appl. Phys.* **1963**, 34, 1793.
- [37] C. J. Barnett, C. Evans, J. E. McCormack, C. E. Gowenlock, P. Dunstan, W. Adams, A. O. White, A. R. Barron, *Nano Lett.* **2019**, 19, 4861.